Journal of Molecular Neuroscience (2025) 75:131
https://doi.org/10.1007/s12031-025-02425-5

RESEARCH

Spinocerebellar Ataxia Type 1 (SCA1) Cell Models Display Widespread Mitochondrial and Extra-Nuclear Alterations

Dane Ford-Roshon[1] · Madison Dudek[1] · Ada Glynn[1] · Abigale Glasman[1] · Jaden York[1] · Emily Lawrence[1] · Donna Nguyen[1] · Lindsay Shinn[1] · Georgia Berry[1] · Lily Kendall[1] · Jennifer Bonner[1,2] · Austin Ferro[1,3] · Sarita Lagalwar[1]

Received: 15 March 2025 / Accepted: 19 September 2025

Abstract

Ataxin-1 (ATXN1) is a nuclear-cytoplasmic shuttling protein, which, when expanded in its polyglutamine coding stretch, causes the progressive neurodegenerative disease Spinocerebellar Ataxia Type 1 (SCA1). While the role of nuclear ATXN1 as a repressor of transcription and regulator of splicing is well studied, its potential cytoplasmic role is more ambiguous. We previously demonstrated mitochondrial dysfunction- including altered respiration and enhanced oxidative stress- is associated with early SCA1 pathogenesis in mice. Moreover, intervention with the electron transport chain substrate succinic acid ameliorated Purkinje cell atrophy and cerebellar behavioral deficits. We now hypothesize that mitochondrial dysfunction in SCA1 may be at least partially due to cytoplasmic interactions between ATXN1 and mitochondria, rather than a result of mutant ATXN1's altered nuclear function. In order to characterize the extent of mitochondrial dysfunction due to mutant ATXN1, we turned to cerebellar-derived Daoy cells which endogenously express human wild type ATXN1. Our SCA1 Daoy model stably over-express phosphorylation-prone, nuclear-aggregating ATXN1[82]. Despite the short lifespan (~ 33 h), Daoy SCA1 cells reveal gross morphological, compositional, and physiological deficits. Conversely, expression in Daoy of a phosphorylation-resistant, cytoplasm-degradable, non-aggregating ATXN1 (ATXN1[82Q-A776]) selectively resulted in intermediate physiological phenotypes and altered mitochondrial protein composition. Finally, our meta-analysis of previously published data supports direct interactions between mutant polyglutamine-expanded ATXN1 and mitochondrial proteins involved in apoptosis, oxidative phosphorylation, composition, and transcription. Our data therefore suggest that irrespective of a disease context and ATXN1[82Q] nuclear aggregation, mitochondrial deficits occur. Overall, the results of this study show mutant ATXN1 can affect metabolic processes outside of its deleterious effect on transcription and splicing, and highlights its multifaceted and multicompartmental function.

Keywords Mitochondrial Dysfunction · Neurodegeneration · Ataxin-1 · Spinocerebellar Ataxia Type 1

Introduction

Spinocerebellar ataxia type 1 (SCA1), a progressive and fatal neurodegenerative disease, primarily affects Purkinje neurons of the cerebellum and brainstem nuclei leading to a host of cerebellar symptoms including uncoordinated movement, gait disturbances, dysarthria, and dysphagia (Schut and Haymaker 1951; Matilla-Dueñas et al. 2008). Previous work has demonstrated that an autosomal dominant polyglutamine expansion mutation in the ataxin-1 (ATXN1) protein causes SCA1 (Orr et al. 1993; Chung et al. 1993; Zoghbi and Orr 2009; Kraus-Perrotta and Lagalwar 2016). ATXN1 is capable of executing various cellular functions through interactions with multiple binding partners (Yue et al. 2001; Chen et al. 2003; Serra et al. 2006; Lim et al. 2008; Lim et al. 2006). The most well-characterized functions of ATXN1 involve the regulation of nuclear processes including RNA transcription, splicing and export. These functions are mediated through direct interactions between ATXN1

✉ Sarita Lagalwar
slagalwa@skidmore.edu

[1] Neuroscience Program, Skidmore College, Saratoga Springs, NY, USA

[2] Biology Department, Skidmore College, Saratoga Springs, NY, USA

[3] Cold Spring Harbor Laboratory, Laurel Hollow, NY, USA

Published online: 02 October 2025

and transcription factors (Lim et al. 2006), splicesomal factors (Lim et al. 2008; Lim et al. 2006; Chiara et al. 2009) and RNA (Yue et al. 2001).

Two modifications of the ATXN1 protein are known to affect its binding interactions, and thus, its nuclear function: polyglutamine expansion within the N-terminal region of the coded protein and post-translational phosphorylation of serine 776 within the C-terminal nuclear localization sequence (Chen et al. 2003; Servadio et al. 1995; Jorgensen et al. 2009). Both modifications enhance ATXN1 stability (Jorgensen et al. 2009; Cummings et al. 1998; Cummings et al. 1999; Park et al. 2013; Perez Ortiz et al. 2018; Lai et al. 2011), increase the likelihood of nuclear aggregation (Jorgensen et al. 2009; Cummings et al. 1998; Cummings et al. 1999; Park et al. 2013; Perez Ortiz et al. 2018; Lai et al. 2011), and alter nuclear binding partner preference (Lim et al. 2008; Chiara et al. 2009).

In cerebellar neurons, ATXN1 shuttles between the cytoplasm and nucleus (Servadio et al. 1995; Irwin et al. 2005). While the cytoplasm has been identified as the site of ATXN1-S776 phosphorylation (Jorgensen et al. 2009; Park et al. 2013; Perez Ortiz et al. 2018; Lai et al. 2011) and ATXN1 stabilization (Chiara et al. 2009; Servadio et al. 1995; Jorgensen et al. 2009; Jorgensen et al. 2007; Cummings et al. 1998, 1999; Lai et al. 2011), the functional role of cytoplasmic ATXN1 within cerebellar cells remain largely ambiguous.

One potential role of cytoplasmic ATXN1 may occur within or regulate the mitochondria. Work from our lab and others have demonstrated the consequence of polyglutamine-expanded ATXN1 expression on mitochondrial function within the cerebellum of mice models. Mice harboring mutant ATXN1 transgenes exhibit mitochondrial DNA damage and depletion (Ripolone et al. 2018; Ito et al. 2015), oxidative stress (Kim et al. 2003) and altered expression of mitochondrial proteins (Ferro et al. 2017a; Ferro et al. 2017b; Stucki et al. 2016; Sanchez et al. 2016). Furthermore, components of the electron transport chain (ETC) are compromised in models with polyglutamine-expanded ATXN1 expression. Multiple studies using diverse polyglutamine expansion lengths, expression levels and sites of expression, report expanded ATXN1 expression mitigates activity through ETC complexes I (Ferro et al. 2017a; Ferro et al. 2017b; Stucki et al. 2016), II (Stucki et al. 2016), III (Ferro et al. 2017a, 2017b; Sanchez et al. 2016), IV (Ripolone et al. 2018; Ferro et al. 2017a, 2017b; Stucki et al. 2016) and V (ATP synthase) (Ito et al. 2015; Stucki et al. 2016). Therapeutic treatment with the mitochondrial-targeting compounds succinic acid (a complex II electron donor) and MitoQ (an antioxidant) alleviate ETC dysfunction (Ferro et al. 2017a, 2017b; Stucki et al. 2016).

One important outstanding question is whether mitochondrial dysfunction is a byproduct of the long course of cellular-, tissue- and organ-level toxicity in SCA1 mice or whether it may be an acute, cell-intrinsic feature of pathology in SCA1 cerebellum. We hypothesize that mutant ATXN1 expression acutely promotes mitochondrial dysfunction in a cell intrinsic manner. To test our hypothesis, we experimentally characterize SCA1 mouse cerebellar tissue and a stably-transfected human cerebellar-derived cell model, Daoy, which has previously been validated to replicate the phosphorylation and stabilization pathways that regulate ATXN1 expression (Park et al. 2013; Perez Ortiz et al. 2018; Huang et al. 2022; Lagalwar 2022). We additionally re-analyze previously published RNA sequencing and transcriptomic datasets in which mitochondrial data had not been explicitly evaluated.

In this study, we provide evidence that cells expressing pathological ATXN1 exhibit widespread and detrimental changes to mitochondrial morphology, localization and function. Furthermore, we show that mitochondrial gene expression is disrupted even when ATXN1 nuclear aggregation is not present. Lastly, we demonstrate that ATXN1 expression leads to altered mitochondrial physiology which can be exacerbated or mitigated through pharmacological targeting of mitochondria. Together, this data suggests that ATXN1 may function in the cytoplasm and mitochondria.

Methods

Meta-Analysis of Genomic and Interatomic Databases

Two publicly available published datasets in which mitochondrial findings were not explicitly evaluated within the original study were utilized in our present study. In the first, (Ingram et al. 2016) shared whole cerebellar RNAseq comparison data from wildtype FVB/n, *ATXN1[30Q-D776]* and SCA1 *ATXN1[82Q-S776]* (B05 line) mice at 5 weeks, 12 weeks and 28 weeks of age. We screened this database for genes involved in mitochondrial function or mitochondrial localization by cross-indexing with the Broad Institute's Mouse MitoCarta 2.0 (www.broadinstitute.org/pubs/MitoCarta). Fold change comparisons of functional mitochondrial genes were graphed in GraphPad Prism.

In the second, (Zhang et al. 2018) conducted an interactomic study to decipher which intracellular proteins mutant ataxin-1 (ATXN1[85Q]) interacted with, or came into proximity with, in N2A cells using a dual approach of proximity-dependent biotin identification and GFP-trap pulldown, under normal and arsenate-stress conditions. We filtered their interactomic data for a sub-list of mitochondrial and glycolytic proteins which bound ATXN1[85Q] through

DAVID Functional Annotation Bioinformatics Analysis (https://david.ncicrf.gov), and by cross-referencing against Mouse MitoCarta 2.0.

Animals

SCA1 B05 transgenic mice on an FVB/nJ background strain were a gift from Dr. Harry Orr (University of Minnesota) (Burright et al. 1995; Burright et al. 1997; Clark et al. 1997; Clark and Orr 2000). B05$^{\pm}$ mice express the *ATXN1[82Q]* transgene under the control of the Purkinje cell-specific promoter *Pcp2/L7* (Burright et al. 1995; Vandaele et al. 1991). Wild type FVB/nJ mice were purchased from Jackson Laboratory (Bar Harbor, ME, 001800). As described previously (Ferro et al. 2017a, 2017b), transgenic mice were bred to homozygosity and maintained along with wild type mice at the Skidmore College mouse facility in strict accordance with the recommendations established for the care and use of laboratory animals by the National Institute of Health and approved by the Skidmore College Institutional Care and Use Committee (IACUC) (*NIH Publications No. 8023, revised 1978).* Heterozygous transgene integration was verified in each generation by PCR. Mice were fed chow ad libitum. Mice were euthanized by displacement of the cage air with 10–30% compressed carbon dioxide gas per minute. Cerebellar hemispheres were dissected out and flash frozen in liquid N_2, prior to permanent storage at −80 degrees C.

Oxidative Stress Assays

Cerebellar hemispheres from SCA1 B05 and FVB/nJ mice were flash-frozen, weighed and stored at −80 degrees C. Samples were thawed on ice prior to use. Reactive oxygen species (ROS)-mediated protein oxidation was assessed with the Protein Carbonyl Content Assay Kit (abcam ab126287). Thawed samples were homogenized and processed following the manufacturer's instructions. Oxidative capacity was assessed with the FRAP (Ferric Reducing Antioxidant Power) Assay Kit (abcam ab234626). Varying dilutions of samples were extracted in acid–methanol solution (methanol:H20:1N HCl at a 70:29.5:0.5 ratio) prior to establishing dilutions that fell within the standard curve range of the assay. Extractions were processed via manufacturer's instructions. Genomic DNA oxidation due to oxidative stress was assessed with the 8-OHdG (8-hydroxy-2'deoxyguanosine) ELISA Kit (abcam ab285254). Samples were homogenized in PBS and processed according to manufacturer's instructions. Data was analyzed on a Biotek ELx808 Absorbance Plate Reader. Protein Carbonyl and FRAP were measured in triplicate from 6 mice per genotype. 8-OHdG was measured from individual samples of 4 mice per genotype. Statistical significance comparing genotypes was determined with an unpaired t-test. *Reflects a p-value of < 0.05.

Cultured Cell Lines

Wild type Daoy human medulloblastoma cells (HTB-186; WT cells) were purchased from American Type Cell Collection; Manassas, MA). Stably-transfected Daoy cells (Park et al. 2013; Huang et al. 2022) expressing *RFP-ATXN1[82Q-S776]-IRES-YFP* (SCA1 cells) or *RFP-ATXN1[82Q-S776A]-IRES-YFP* (ATXN1[82Q-A776] cells) were a generous gift from the Zoghbi lab at Baylor College of Medicine. All cell lines were maintained in DMEM-high glucose (4.5 g/L) media supplemented with 10% fetal bovine serum, 1% penicillin/streptomycin, and 1% L-glutamine at 37℃/5% CO_2.

Transmission Electron Microscopy

In order to image mitochondrial ultrastructure in cultured cells, confluent plates of Daoy cells were pelleted, washed with PBS and fixed by re-suspending in fresh 2.5% glutaraldehyde/PBS, pH 7.0, for four hours. Following fixation, cells were washed in PBS three times and re-pelleted. Electron density and contrast was enhanced by treating the cell pellets with 1% osmium tetroxide/PBS, pH 7.0 for two hours at 4 ℃. Post-secondary fixation, cells were washed and re-pelleted.

Pellets were then dehydrated sequentially for 30 min each in 10%, 25%, 50%, 75%, 90% and 100% ethanol/PBS solution, prior to embedding in fresh Spurr's plastic resin using the Spurr Low-Viscosity Embedding Kit. The Spurr resin was allowed to polymerize for 48 h at 60 ℃.

Sections varying in thickness from 60–90 nm were sliced on a Leica EM UC6 microtome and collected onto nickel-plated mesh transmission electron microscopy grids under puffs of chloroform gas to reduce wrinkling. Sections were allowed to dry on grids overnight.

Grids were stained with 1% uranyl acetate/deionized water for 5–30 min, washed with boiled CO_2-free deionized water and dried, prior to staining with lead citrate solution for 45 s to 2 min. Immediately following staining, grids were dipped in boiled deionized water, rinsed in room temperature deionized water, dried for 12 h and imaged on a Zeiss Libra 120 Transmission Electron Microscope.

Live Cell Imaging with JC-10 and Fluo-4AM

Mitochondrial membrane potential measurements were performed by incubation with JC-10 dye (Ion Biosciences Ion Vital MitoVolt #5100) according to manufacturer's instructions. Upon addition of the masking solution, 1 µM staurosporine (STR), 600 nM rotenone or DMSO vehicle

was added to wells for up to 3 h, or 3.4 µM succinic acid was added overnight, in order to induce alterations in mitochondrial dynamics. The green and red JC-10 signals were captured on an EVOS imaging station using GFP and RFP filters. Additionally, the Olympus inverted Fluoview 3000 was used to image JC-10/STR-treated cells in real-time in a 37℃/5% CO_2 chamber. Z-stack images were captured at a single location prior to the addition of masking solution, following the addition of masking solution, and every 10 min following the addition of 1 µM STR for a total of 80 min. Fluoview software was used to measure real-time changes in green and red channel signals over time from individual whole cells, and that data was processed using Fiji software. Calcium influx was imaged with Fluo-4AM Ca^{2+} indicator dye (Ion Biosciences #1041F) and the addition of pluronic F-127 solution (Ion Biosciences #7601A) according to manufacturer's instructions following treatment with DMSO vehicle or 1 µM STR for 3 h. Fluo-4AM images were captured on the EVOS using GFP filters. All JC-10 and Fluo-4AM were repeated at least six times in independent experiments. Results shown are of all cells measured from an individual, replicative, experiment.

Immunocytochemistry and Confocal Microscopy

Immunocytochemistry of cultured Daoy cells was performed as previously described (Huang et al. 2022). Specifically, harvested cells were plated at a concentration of 5000 cells per well in 8-well chamber slides (Lab Tek II) and allowed to grow for 2 days. Cells were fixed in ice cold methanol solution (10% MES Buffer (100 mM MES, pH 6.9, 1 mM EGTA, 1 mM $MgCl_2$), 90% methanol) for 5 min on ice, washed with PBS, and blocked with 3% goat serum/0.5% Triton X-100/PBS for 15 min. Primary antibody (see antibody dilution table) was added for 3 h at 37℃, and washed off. Secondary antibodies were added for either 1 h at 37℃ or overnight at 4℃. DAPI nuclear stain was added via ProLong Gold antifade mounting medium (ThermoFisher P36931). Fluorescent images were taken on the EVOS Cell Imaging System. Single plane images and three-dimensional Z-stacks (11–14 sections, 20 µm thick stack) were taken on the Olympus/Evident Fluoview 1200 Laser Scanning confocal microscope.

Tom20 and MfN2 staining were analyzed and quantified using an Olympus BX63 upright fluorescent light microscope. Mean intensities within individual cells from 6–9 regions per genotype/antibody across three or four independent culturing and staining experiments were recorded. Background intensity was subtracted in order to calculate corrected raw intensity scores which were averaged and graphed, along with standard error around the mean, in Graph Pad Prism. Statistical significance was determined by one-way ANOVA with Tukey's multiple comparisons post-hoc analysis. *Reflects a p-value < 0.05 and **** reflects a p-value < 0.0001 (Table 1).

ATP and ROS luciferase Assays

ATP levels were detected in WT Daoy and ATXN1[82Q] cells using the Luminescent ATP Detection Assay kit (abcam ab113849). Harvested cells were plated at a concentration of 5000 cells per well in 8-well chamber slides (Lab Tek II) and allowed to grow under normal conditions for 2 days. ATP stabilization, cell lysing, substrate addition and substrate development were performed according to manufacturer's instructions. Following dark adaptation, samples were transferred to 12 × 75 mm Luminescene tubes and relative luminescence units (RLU) were detected on a Junior LB 9509 Portable Luminometer (Berthold Technologies, Oak Ridge, TN). To account for differences in growth rates, RLU values were normalized to a Daoy: ATXN1[82Q] differential growth ratio of 1.3, and percent of control was calculated and graphed in Graph Pad Prism.

Hydrogen peroxide, a form of reactive oxygen species (ROS) with a long half-life, was measured in WT Daoy and ATXN1[82Q] cells using the ROS-Glo H_2O_2 Assay kit (Promega G8820). Harvested cells were plated at a concentration

Table 1 Antibody dilution table

Antibody	Target	Species	Source	Dilution
11NQ	ATXN1 N-terminus	Rabbit	Orr lab, University of Minnesota	1:500
Anti-TOM20 IgG1	Tom20 protein, mitochondrial TOM complex (EPR15581-39)	Mouse	abcam a#b283317	1:250
Anti-Mfn2	Mitofusin-2 (D1E9)	Rabbit	Cell Signaling Technology #11925	1:250
Mitofilin (anti-Mic60)	Mic60 protein, MICOS complex (2E4AD5)	Mouse	abcam #ab110329	1:250
Anti-Opa1	Optic atrophy protein 1, mitochondrial dynamin-like GTPase (FLJ12460)	Rabbit	Cell Signaling Technology #80471	1:250
Anti-rabbit IgG-Alexa 594	Rabbit IgG	Goat	Cell Signaling Technology #8889	1:250
Anti-mouse IgG-FITC	Mouse IgG	Mouse	Life Technologies #F276	1:250
Anti-rabbit IgG-Alexa 488	Rabbit IgG	Goat	Cell Signaling Technology #4412	1:250

of 3000 Daoy cells or 5000 ATXN1[82Q] cells, to account for the difference in growth rates, in 8-well chamber slides and allowed to grow for 2 days in regular growth media (25 mM "high" glucose) or glucose-free DMEM (Thermo Fisher 11966025) supplemented with 10 mM "high" galactose. Treatment was performed by adding 500 nM MitoQ in DMSO, DMSO vehicle, or varying doses of succinic acid (0.0034–3.4 mM) in deionized water, for 24 h with incubation at 37℃ with 5% CO_2. Following manufacturer's instructions, substrate solution was added for 6 h and detection solution was added for 20 min prior to transferring samples to 12 × 75 Luminescene tubes and detection of RLU values on the luminometer. RLU values were normalized to a Daoy: ATXN1[82Q] differential growth ratio of 1.3, and percent of control was calculated and graphed in Graph Pad Prism.

Statistical significance was determined by one-way ANOVA and Tukey's multiple comparisons post-hoc analysis. * Reflects a p-value < 0.05, ** reflects a p-value < 0.01, and *** reflects a p-value < 0.005.

Seahorse Mito Stress Test

Oxidative phosphorylation and glycolysis rates in Daoy, ATXN1[82Q] and ATXN1[82Q-A776] cells were measured on the Seahorse XFe96 Bioanalyzer (Agilent Technologies, Santa Clara, CA) using the Mito Stress Test Assay kit. Cells were harvested and plated in triplicate at a concentration of 20,000 cells per well overnight. Following manufacturer's instructions, 1.0 mM oligomycin, 1.0 mM FCCP and 0.5 mM rotenone/antimycin A were prepared and added to the culture plate reservoirs for addition in real-time at 20 min, 40 min and 60 min, respectively, during the 75-min assay. Following completion, NucBlue Live ReadyProbes Reagent (Invitrogen R37605) was added to the wells for 10 min in order to identify live cells across the three cell lines, and ratios were used to normalize the final results by cell growth rates. Data analysis was conducted by Wave software (Agilent Technologies) and Graph Pad Prism. The Mito Stress Test assay was conducted in three independent experiments, and the results presented are from one representative experiment.

Results

Mutant ATXN1[82Q] expression alters mitochondrial protein expression in mouse cerebellar tissue. Our lab and others (Ripolone et al. 2018; Ferro et al. 2017b; Stucki et al. 2016) previously demonstrated mitochondrial OXPHOS deficits in cerebellar tissue of SCA1 mice models preceded disease pathology and symptom onset. In order to gauge whether functional mitochondrial genes apart from the electron transport genes are altered in SCA1 cerebellum, we conducted a meta-analysis by cross-referencing the Ingram et al. (Ingram et al. 2016) SCA1 RNAseq dataset with the *MitoCarta 2.0* database. The Ingram dataset contained genes from whole cerebellar tissue of 5-, 12-, and 28-week FVB/n wild type (WT) mice, ATXN1[82Q-S776] (Progressive SCA1, B05 line) mice, and ATXN1[30Q-D776] (Non-progressive SCA1) mice. At the time of our meta-analysis, the MitoCarta2.0 database consisted of 1158 mouse genes experimentally determined to exhibit mitochondrial function. A subfraction of 27–32 genes showed differential expression in the Progressive or Non-progressive SCA1 cerebellar tissue compared to WT cerebellar tissue, with a total of 40 genes (3.5%) showing differential expression at one or more developmental ages (Fig. 1A).

The most obvious feature of our meta-analysis is the increased expression of genes in the Progressive or Non-progressive SCA1 tissue compared to WT, with only a small number of genes showing decreased expression. Among the latter are Casp3 (NCBI Ref Seq NM_001284409.1; caspase-3), the execution-phase apoptotic cysteine-aspartic acid protease, which shows greater downregulation in Progressive SCA1 than Non-progressive SCA1. Aldh9a1 (NM_019993.4; aldehyde dehydrogenase 9, subfamily A1), an electron acceptor enabling oxidoreductase activity, shows similar and slight downregulation in both the Progressive and Non-progressive SCA1 compared to WT at 12 weeks of age.

The sodium/glucose co-transporter gene Slc5a1 (NM_019810.4) and centrosomal proteins Cep72 (NM_028959) and Cep76 (NM_001081073) show elevated expression levels in Non-progressive SCA1 mouse cerebellum compared to WT, with the highest expression apparent at 12 weeks. In contrast, the transmembrane protein Tmem255a (NM_172930) shows elevated, but decreasing expression with age, while the hexokinase Hk2 (NM_013820) shows elevated, but increasing expression with age (Fig. 1A).

The guanine nucleotide binding protein Gng13 (NM_022422), Fam107b (NM_025626), sodium/proton exchanger Slc9a3 (NM_001081060), and cytochrome c oxidase subunit Cox6b2 (NM_183405) show greater expression in Progressive SCA1 mouse cerebellum compared to WT. Of those, Gng13 and Slc9a3 increase with age, Fam107b shows highest levels of expression at 12 weeks, and Cox6b2 decreases with age (Fig. 1B). Overall, the results of our meta-analysis show substantial differential regulation of expression of multiple functional mitochondrial genes, beyond just those involved in oxidative phosphorylation.

ATXN1[82Q] expression in SCA1 mice cerebellum produces features of selective oxidative stress. Previously, we identified oxidative phosphorylation chain complex I dysfunction in whole cerebellar tissue from B05 mice (Ferro et al. 2017b). We now verify that selective measures of

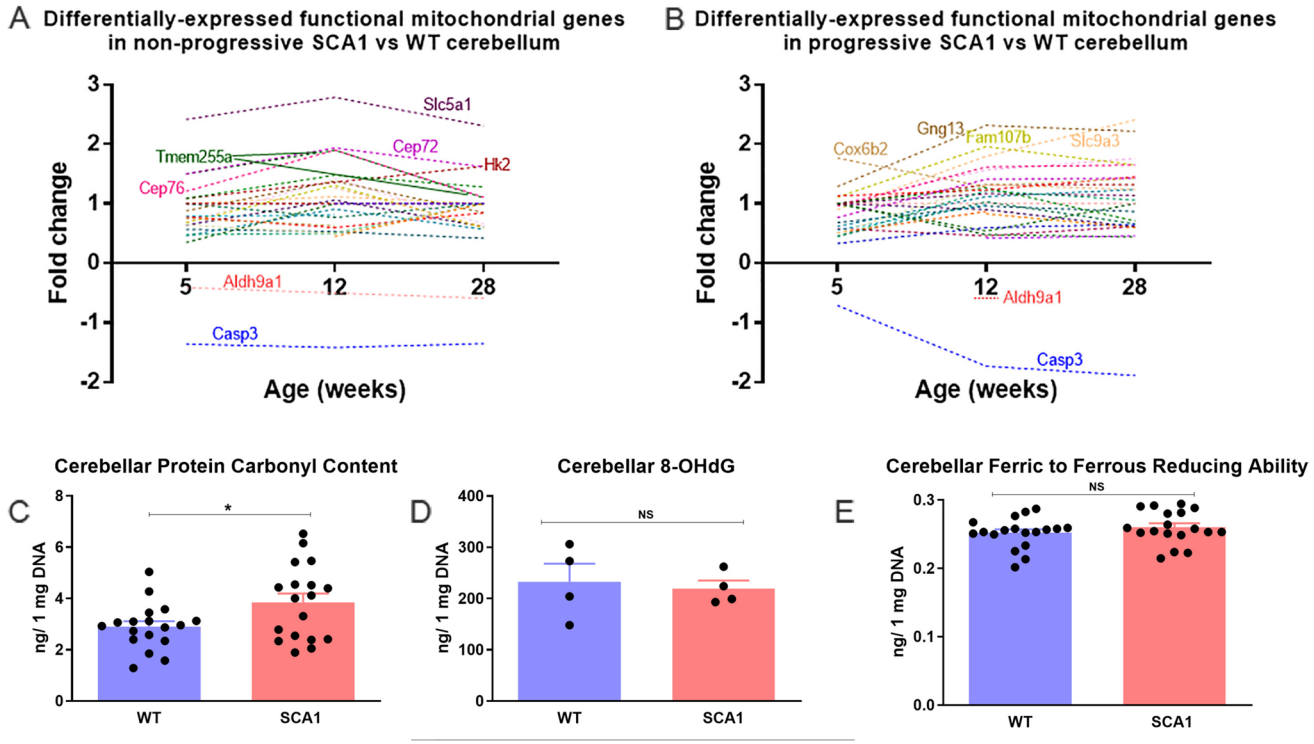

Fig. 1 Mutant ATXN1 expression in cerebellar Purkinje neurons selectively alters nuclear-encoded mitochondrial gene expression and oxidative stress in cerebellar tissue. A-B) Datasets displaying genes with significant differential expression between Progressive SCA1 and WT, and between Non-progressive SCA1 and WT in cerebellar tissue were re-analyzed. Graphed are differential expression ratios of *MitoCarta2.0*/Ingram et al. genes in cerebellar tissue from ATXN1[30Q-D776] (Non-progressive SCA1) mice compared to WT mice **A** and ATXN1[82Q-S776] (Progressive SCA1, B05 line) mice compared to WT mice **B** at 5, 12 and 28 weeks of age (x-axis). (C-E) SCA1 mice cerebellar tissue displays selective forms of oxidative stress; specifically, increased protein carbonylation **C**, but not DNA oxidative damage **D** or reducing ability **E**. *$P < 0.05$

oxidative stress are increased compared to WT cerebellar tissue. Protein carbonylation, a form of protein oxidation promoted by ROS generation, is significantly elevated in SCA1 (3.849 ± 0.3422 nmol per mg tissue) compared to WT (2.902 ± 0.2104 per mg tissue) ($p < 0.05$) (Fig. 1C). However, no difference in oxidative DNA damage (B05: 219.5 ng $\pm$ 15.68 ng per mg genomic DNA; WT: 227.0 ± 79.00 ng per mg genomic DNA; $P = 0.8958$) (Fig. 1D) or oxidative capacity (B05: 0.2524 ± 0.0022 mmol FeSO4; WT: 0.2491 ± 0.0079 mmol $FeSO_4$; $P = 0.6934$) (Fig. 1E) was detected. Taken together, these results indicate that expression of ATXN1[82Q] protein in cerebellar Purkinje neurons produces select cytoplasmic metabolic deficits.

ATXN1[82Q] expression produces cytoplasmic physiological deficits in SCA1 cell models. We next assessed whether expression of the ATXN1[82Q] transgene in cerebellar-derived cell models of SCA1 correlates with cytoplasmic deficits. We used a Daoy line, a human medulloblastoma cell which endogenously expresses ATXN1, in which RFP-ATXN1[82Q] is stably expressed (Park et al. 2013; Huang et al. 2022; Lagalwar 2022) (SCA1 cells). First, we measured ATP levels in WT ($100.0 \pm 7.284\%$) and SCA1 cells ($25.73 \pm 1.598\%$) under resting conditions and found that SCA1 cells featured a statistically decreased amount of ATP production ($P < 0.0001$) (Fig. 2A). Oxidative stress in the form of the cell permeable ROS H_2O_2, under resting conditions, was measured next. WT cells exhibited a non-significant trend of reduced H_2O_2 production (by $75.92 \pm 7.622\%$) compared to SCA1 cells (Fig. 2B). Whole cell calcium activity of SCA1 cells compared to WT cells (Fig. 2C-E) was significantly increased ($P < 0.0001$). Moreover, application of 1 µM STR for 3 h evoked a strong calcium response in SCA1 cells (Fig. 2G) compared to WT cells (Fig. 2F), exhibited by increased signal intensity (Fig. 2G). Taken together, these results show that under resting conditions, expression of ATXN1[82Q] produces cytoplasmic physiological deficits and suggest that Daoy cells may be a good model for studying those deficits in the context of SCA1.

ATXN1[82Q] expression produces mitochondrial morphological and localization deficits in SCA1 cells. In order to determine whether ATXN1[82Q] expression affects mitochondrial morphology, we visualized their ultrastructure in WT and SCA1 cells (Fig. 3A-D). WT mitochondria

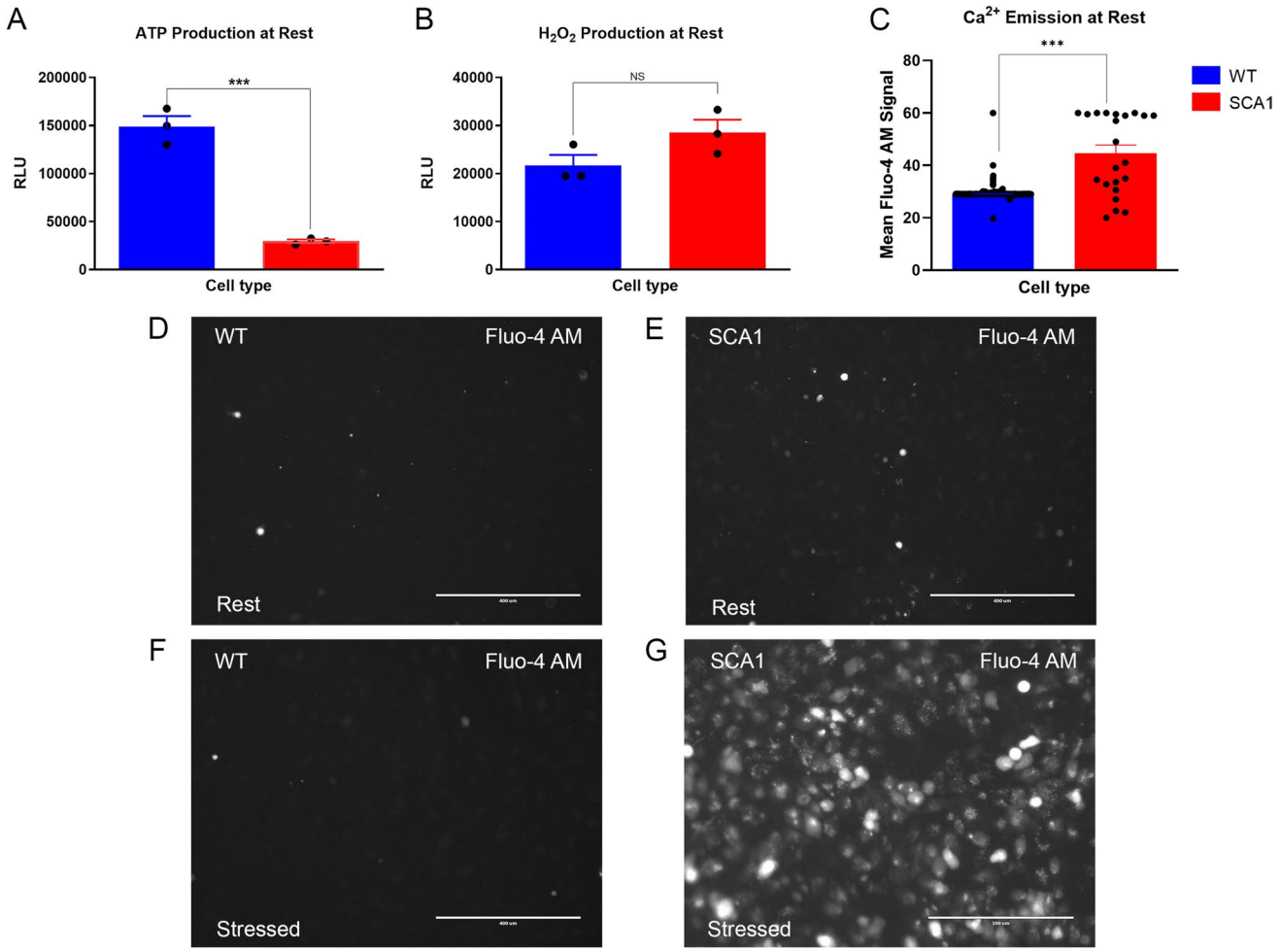

Fig. 2 Mutant ATXN1 expression in cerebellar-derived Daoy cells alters cellular physiology. **A** During rest conditions, SCA1 cell models expressing RFP-ATXN1[82Q] and endogenous ATXN1 display decreased ATP production compared to WT Daoy cells. **B** During rest conditions, SCA1 cell models display increased H_2O_2 ROS production compared to WT Daoy cells. **C**-**E** During rest conditions, SCA1 cell models **D** display increased GFP fluorescence of the calcium indicator dye Fluo-4AM compared to WT Daoy cells **E**. Following 3 h of cellular stress instigation with 1 µM STR **F**-**G**, SCA1 cells **G** selectively feature enhanced $Ca.^{2+}$ granule formation, compared to WT cells **F**. *** $P < 0.001$

appear oval-shaped with intact outer membrane and cristae stretched through the organelle (Fig. 3A). SCA1 mitochondria, in contrast, feature rounded morphology, vacuoles and disrupted cristae (Fig. 3B-D). To visualize alterations in mitochondrial localization, we labeled the MICOS complex Mic60 subunit using Mitofilin (green) (Fig. 3E). RFP-ATXN1[82Q] and endogenous ATXN1 were labeled with the 11NQ polyclonal antibody (red). Large aggregates of RFP-ATXN1[82Q]/ATXN1 appear primarily nuclear (DAPI). However, smaller aggregates and more diffuse protein appear cytoplasmic. Notably, when nuclear aggregates are present, mitochondria display perinuclear localization (Fig. 3E). Next, RFP-ATXN1[82Q-A776] and endogenous ATXN1 were labeled with 11NQ antibody (red), Mic60 (green), and DAPI (blue) (Fig. 3F). In contrast to SCA1 cells (Fig. 3E), ATXN1[82Q-A776] cells retained diffuse nuclear ATXN1, likely endogenous, and diffuse mitochondrial Mic60 throughout the cytoplasm. These results indicate gross, widespread mitochondrial changes in SCA1 cells caused by expression of the disease-prone ATXN1[82Q] protein.

ATXN1[82Q] expression alters mitochondrial protein production in SCA1 cells. To assess whether mitochondrial protein levels are affected by expression of RFP-ATXN1[82Q], we compared the inner mitochondrial membrane protein Optic Atrophy 1 (OPA1), the mitochondrial fusion regulator Mitofusion2 (MFN2), and the mitochondrial import protein TOM20 in the three cell lines. Compared to WT cells (Fig. 4A) or ATXN1[82Q-A776]-expressing cells (Fig. 4B), OPA1 expression (green)

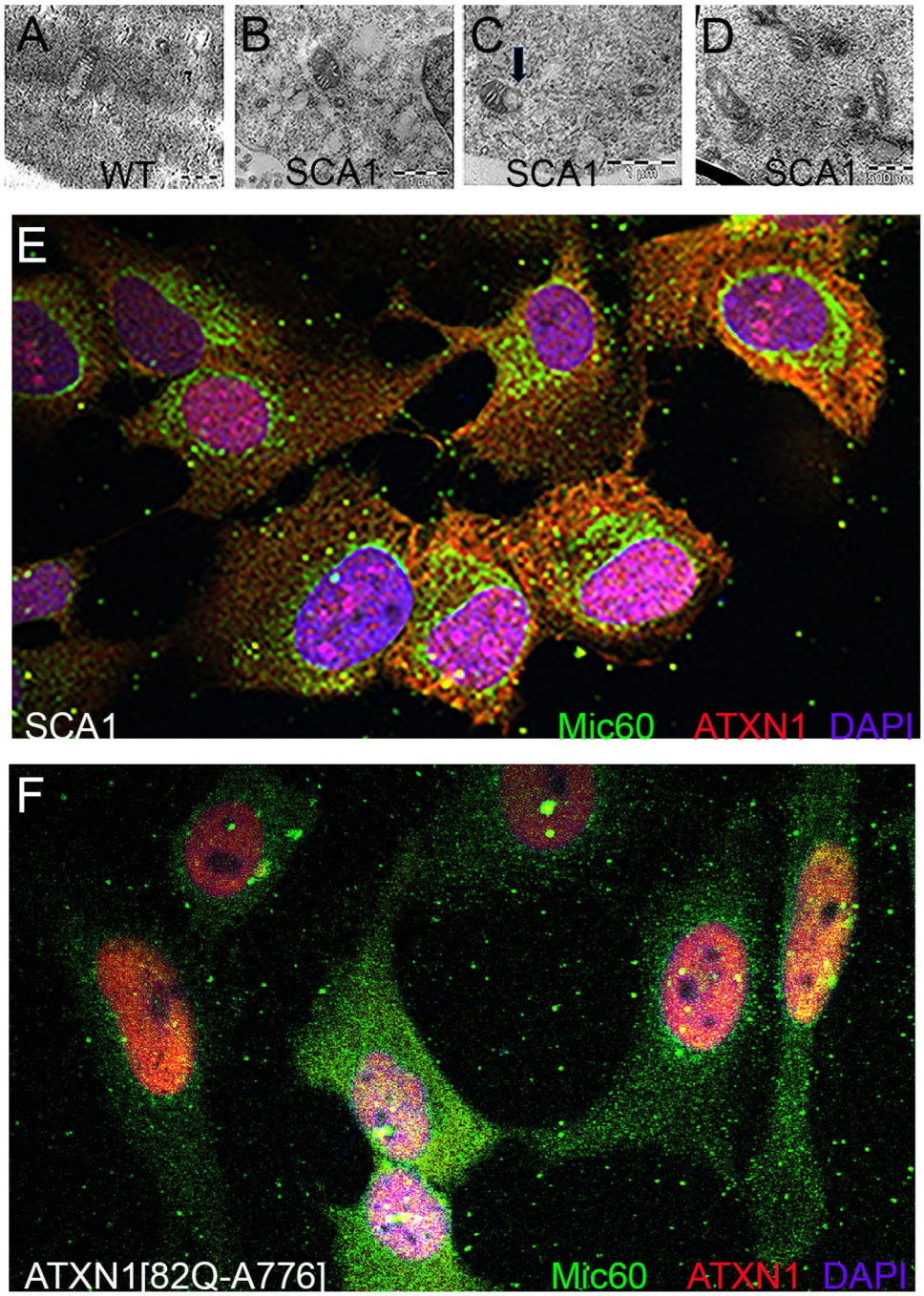

Fig. 3 Mutant ATXN1 expression in cerebellar-derived Daoy cells disrupts mitochondrial morphology and localization. **A**-**D** Transmission electron micrograph (TEM) imaging of mitochondria in WT cells **A** and SCA1 cells **B**-**D**. SCA1 mitochondria are distorted with cristae disruptions, large vacuoles and a rounded morphology. **E** RFP-ATXN1[82Q] (red) stained for Mitofilin/Mic-60 (green) display perinuclear mitochondrial localization when ATXN1 nuclear aggregates are present. **F** RFP-ATXN1[82Q-A776] (red) stained for Mitofilin/Mic-60 (green), display nuclear diffuse ATXN1 and cytoplasmic mitochondrial localization

displays decreased diffuse, cytoplasmic expression in SCA1 cells and instead localizes perinuclearly, as shown against the blue nuclear DAPI stain (Fig. 4C-D).

In contrast, protein expression analysis of MFN2 and TOM20 reveals decreased levels of both proteins in the transgenic lines compared to WT cells (Fig. 4E). Specifically, one-way ANOVA of MFN2 expression in the three cell lines [$F\ (2, 177) = 12.67$, $p < 0.0001$] shows no significant difference in expression levels between SCA1 and ATXN1[82Q-A776] cells (normalized mean value of 73.34 and 75.11, respectively; Tukey's post hoc analysis $p = 0.9521$). However, significant decreases in expression are found between SCA1 and WT cells (normalized mean value of 73.34 and 100.00, respectively; Tukey's post hoc analysis $p < 0.0001$) and between ATXN1[82Q-A776] and WT cells (normalized mean value of 75.11 and 100.00, respectively; Tukey's post hoc analysis $p = 0.0001$).

One-way ANOVA of TOM20 [$F\ (2, 237) = 14.62$, $p < 0.0001$] shows no significant difference in expression between SCA1 and ATXN1[82Q-A776] cells (normalized

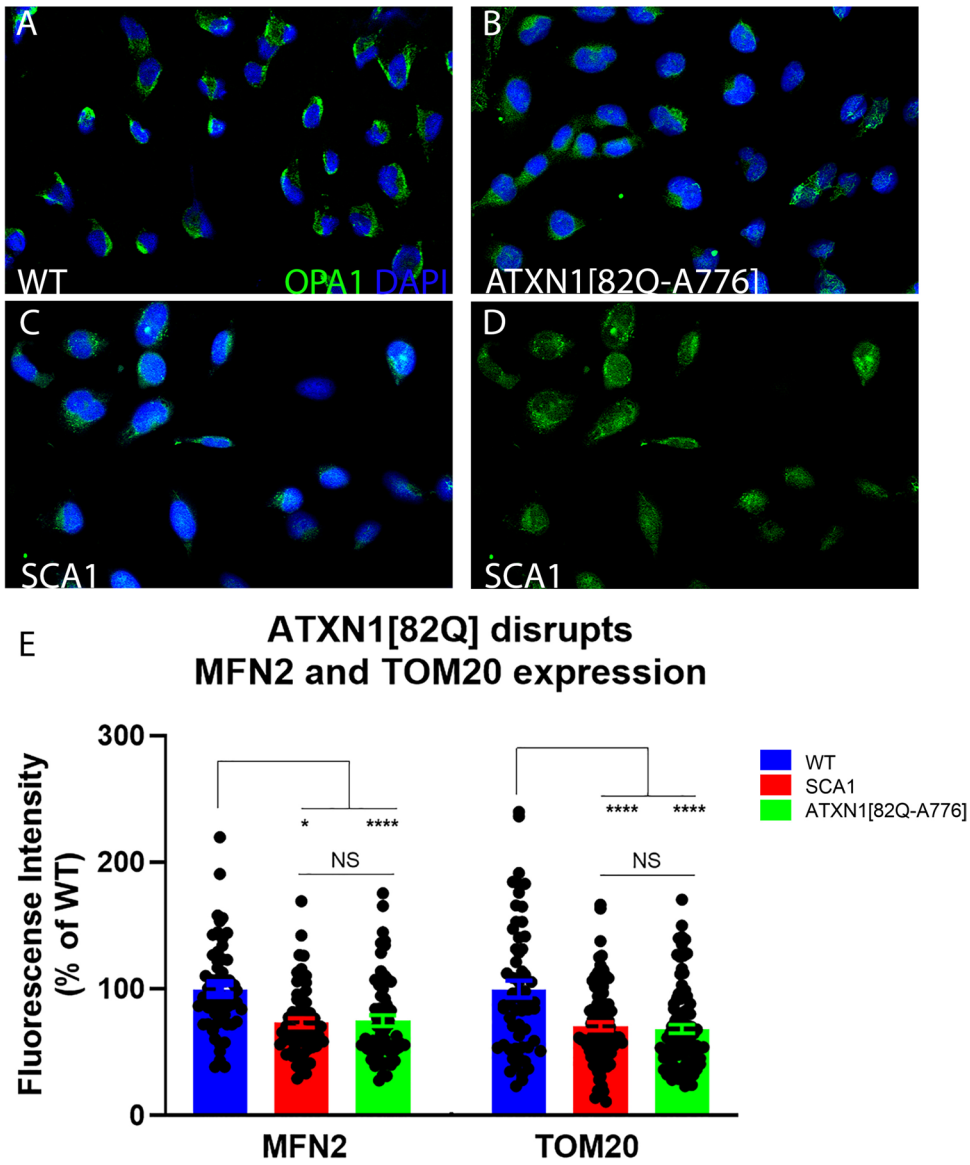

Fig. 4 Mutant ATXN1 expression in cerebellar-derived Daoy cells alters mitochondrial protein expression. **A**-**D** Cytoplasmic dynamin-related GTPase OPA1 (green) displays greater levels of cytoplasmic expression in WT **A** and RFP-ATXN1[82Q-A776] **B** cells than in SCA1 cells **C**-**D**. DAPI nuclear staining is shown in blue. (E) Protein expression of mitofusin 2 (MFN2) and TOM20 is decreased in cells expressing ATXN1[82Q] transgenes compared to WT cells. * $P < 0.05$, **** $P < 0.0001$

mean value of 70.67 and 68.50, respectively; Tukey's post hoc analysis $p = 0.9216$). Similarly, significant decreases in expression are found between SCA1 and WT cells (normalized mean value of 70.67 to 100.00, respectively; Tukey's post hoc analysis $p < 0.0001$) and between ATXN1[82Q-A776] and WT cells (normalized mean value of 68.50 to 100.00, respectively; Tukey's post hoc analysis $p < 0.0001$).

The results of Fig. 4 indicate differential regulation of mitochondrial proteins in the presence of ATXN1[82Q] and ATXN1[82Q-A776]. While OPA1 expression is selectively altered in SCA1 cells compared to WT and ATXN1[82Q-A776], MFN2 and TOM20 are equally affected in the presence of both transgenic ATXN1 polyglutamine-expanded proteins, regardless of their phosphorylation status. Importantly, the selective alteration of mitochondrial gene expression by ATXN1[82Q-A776] in particular, which cannot be phosphorylated at the 776 residue and therefore is not readily nuclear-translocated, indicates that it is *cytoplasmic* ATXN1 that is causing the disruption.

ATXN1[82Q] expression alters mitochondrial physiology in SCA1 cell models. We next assessed energy metabolism and oxidative phosphorylation. SCA1 cells display higher extracellular acidification rates (ECAR, a measure of cellular glycolysis) and higher oxygen consumption rates (OCR, a measure of mitochondrial oxidative phosphorylation) than WT cells, pushing them into an "energetic" phenotype indicative of cellular stress. Interestingly, cells stably expressing ATXN1[82Q-A776] display a phenotype in-between the WT and SCA1 models (Fig. 5A). Notably, ATXN1[82Q-A776] cells also display intermediate levels of basal respiration

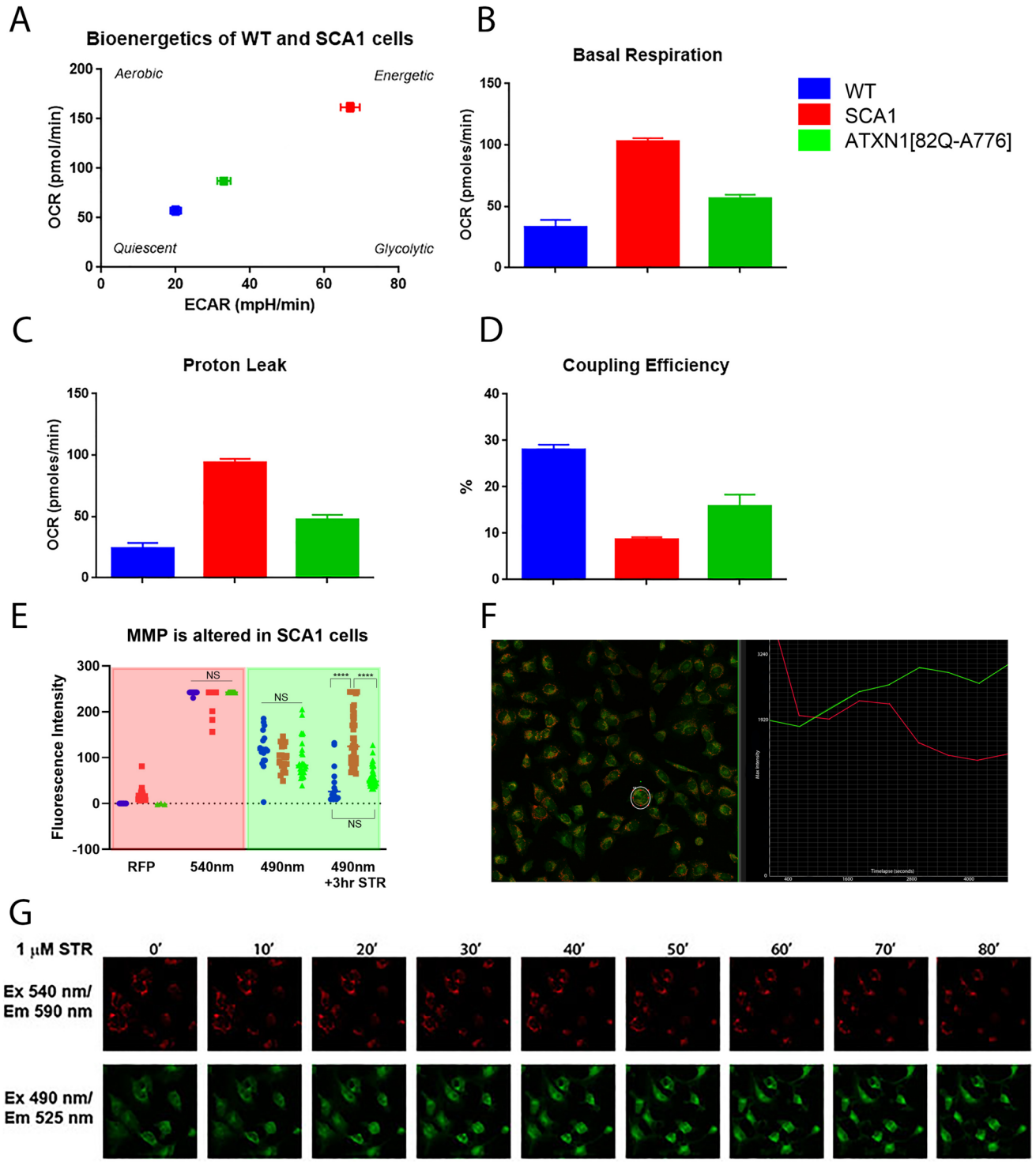

(Fig. 5B), proton leak (Fig. 5C) and coupling efficiency (Fig. 5D). The low coupling efficiency of SCA1 cells, which is a measure of the percentage of respiration used for ATP synthesis, appears in line with low ATP levels (Fig. 2A).

Finally, we assessed mitochondrial membrane potential (MMP) by its green:red ratio, a measure of overall mitochondrial health. Importantly, RFP levels in the SCA1 cells (mean intensity = 17.33) were lower than the 540 nm red channel emittance (mean intensity = 236.9) and did not affect the MMP signal of SCA1 cells. Under resting conditions, WT, SCA1 and ATXN1[82Q-A776] cells emitted statistically similar levels of red (mean intensities = 241.3, 236.9, 242, respectively; [$F(2, 84) = 1.766$, $p = 0.1773$]) and green (mean intensities = 118.7, 98.25,

◂**Fig. 5** Mutant ATXN1 expression in cerebellar-derived Daoy cells alters mitochondrial physiology. **A** WT cells display low bioenergetics, measured by the Seahorse MitoStress test, indicative of a quiescent state compared to the high bioenergetics displayed by SCA1 cells, indicative of an energetic, stressed state. In contrast, ATXN1[82Q-A776] cells display intermediate extracellular acidification rate (ECAR) and oxygen consumption rate (OCR) phenotypes **C**, indicative of an in-between state. The energy map data is reflective of the SCA1 cells having higher basal respiration levels **B**, enhanced proton leak **C** and decreased ATP production coupling efficiency **D** than WT cells, with ATXN1[82Q-A776] cells again displaying intermediate phenotypes. **E** Red channel and green channel mitochondrial membrane potential emission from individual WT cells, SCA1 cells and ATXN1[82Q-A776] cells following loading with JC-10 dye and masking solution was imaged and quantified. Of note is the inclusion of RFP-tagged-ATXN1[82Q] and RFP-tagged-ATXN1[82Q-A776] in the red channel emission. Cells were next treated with 1 µM STR, imaged after three hours, and their green channel emission were plotted. **F-G** Time-lapse imaging following specific JC-10-loaded ATXN1[82Q] cells over eighty minutes of STR treatment shows a gradual decrease in red channel emission and a gradual increase in green channel emission, indicative of depolarizing mitochondrial membrane potential. **F** Red and green emission traces from a single RFP-ATXN1[82Q] cell (shown with white circle) over time following STR treatment. **** $P < 0.0001$

95.24, respectively; [F (2, 64) = 2.324, $p = 0.1061$] fluorescence (Fig. 5E).

We next measured the response to STR-induced cellular stress. Treated SCA1 cells featured increased green wavelength emission (mean intensity = 144.3) compared to treated WT (mean intensity = 43.21) or treated ATXN1[82Q-A776] cells (mean intensity = 56.10). One-way ANOVA analysis confirmed the statistical increase in the green MMP emission from treated SCA1 cells [F (2, 104) = 55.67, $p < 0.0001$] (Fig. 5E, 3 hr STR). Tukey's post hoc analysis p-values between WT and SCA1 cells ($p < 0.0001$), between SCA1 and ATXN1[82Q-A776] cells ($p < 0.0001$), and between WT and ATXN1[82Q-A776] cells further confirm that only the SCA1 line displayed mitochondrial vulnerability to cellular stress.

In order to visualize the change in SCA1 cells during stress induction, we used time-lapse imaging to calculate maximum emission from an individual whole z-stacked SCA1 cell (white circle) over 80 min post-induction (Fig. 5F). The graph in Fig. 5F shows decreased red channel emission and the corresponding increased green channel emission during that time period (Fig. 5F). To visualize population changes, field images were taken at 540 nm and 490 nm every 10 min (Fig. 5G). The visual reduction in red signal and corresponding increase in green signal can be seen in Fig. 5G.

The results of Fig. 5 support that mitochondrial physiology is altered in the presence of mutant ATXN1. Taken together, the results of Figs. 2, 3, 4 and 5 indicate that widespread cytoplasmic and mitochondrial morphological, biochemical and physiological changes occur in SCA1 cell models in the presence of mutant ATXN1[82Q] expression.

Does cytoplasmic ATXN1[82Q] directly contribute to mitochondrial dysfunction? We addressed this question in the following ways. First, we investigated whether mitochondrial-targeted compounds alter the physiological deficits induced by the expression of ATXN1[82Q]. Increased ROS H_2O_2 is increased in SCA1 cells compared to WT cells at rest (Fig. 2B). Moreover, the electron transport chain complex II substrate, succinic acid, significantly decreased H_2O_2 ROS levels (67.1667 ± 7.640%); $p < 0.05$) (Fig. 6A). Increases in concentrations up to 3.4 mM resulted in greater decreases in H_2O_2 ROS levels (0.034 mM: 57.576 ± 0.599%; 0.34 mM: 58.170 ± 3.400%; 3.4 mM: 57.990 ± 1.515%; all: $p < 0.01$) (Fig. 6A).

We next measured the production of ROS H_2O_2 in SCA1 cells in the presence of the mitochondrial-selective antioxidant, MitoQ (Stucki et al. 2016), under either high (25 mM) glucose conditions or high (10 mM) galactose conditions (Fig. 6B). MitoQ reduced H_2O_2 production in SCA1 cells (68.67 ± 11.76%; $P < 0.05$) (Fig. 6B) compared to WT levels under high glucose conditions. Under high galactose conditions, 500 nM MitoQ increased H_2O_2 production in SCA1 cells (132.3 ± 4.133%) compared to WT cells (100.0 ± 3.783%; $P < 0.001$) (Fig. 6B), perhaps due to compensation in the context of enhanced elimination during high metabolism.

Finally, we measured mitochondrial membrane potential in vehicle-treated WT and SCA1 cells, and SCA1 cells treated with the complex I inhibitor rotenone, succinic acid, or both [F (4, 627) = 35.02, $p < 0.0001$]. The MMP green:red ratio of SCA1 cells (n = 180, mean ratio = 0.4732 ± 0.03; Fig. 6C, 6E) to WT cells (n = 90, mean ratio = 0.2290 ± 0.01; Fig. 6C-D) was calculated. Significant differences between the SCA1 to WT ratios were determined by post hoc analysis ($p < 0.0001$). Treatment of SCA1 cells with 600 nM rotenone for 3 h (n = 122, mean ratio = 0.6845 ± 0.03; Fig. 6C, 6F) caused an increase in the MMP ratio compared to vehicle treatment (post hoc analysis of $p < 0.0001$). In contrast, the overnight addition of 3.4 µM succinic acid to SCA1 cells (n = 120, mean ratio = 0.3911 ± 0.03; Fig. 6C, 6G) did not significantly alter the MMP ratio ($p = 0.1108$). Overnight pre-treatment with 3.4 µM succinic acid prior to adding rotenone (n = 120, mean ratio = 0.4386 ± 0.02; Fig. 6C, 6H) significantly reduced the MMP ratio compared to rotenone-treatment alone ($p < 0.0001$). No significant difference was calculated between succinic acid/rotenone-treated SCA1 cells and succinic acid-treated SCA1 cells ($p = 0.7048$).

The results of Fig. 6 suggest that alteration of mitochondria by enhancing electron transport chain function with succinic acid, or neutralizing mitochondrial reactive oxygen species with MitoQ, can mitigate the enhanced oxidative

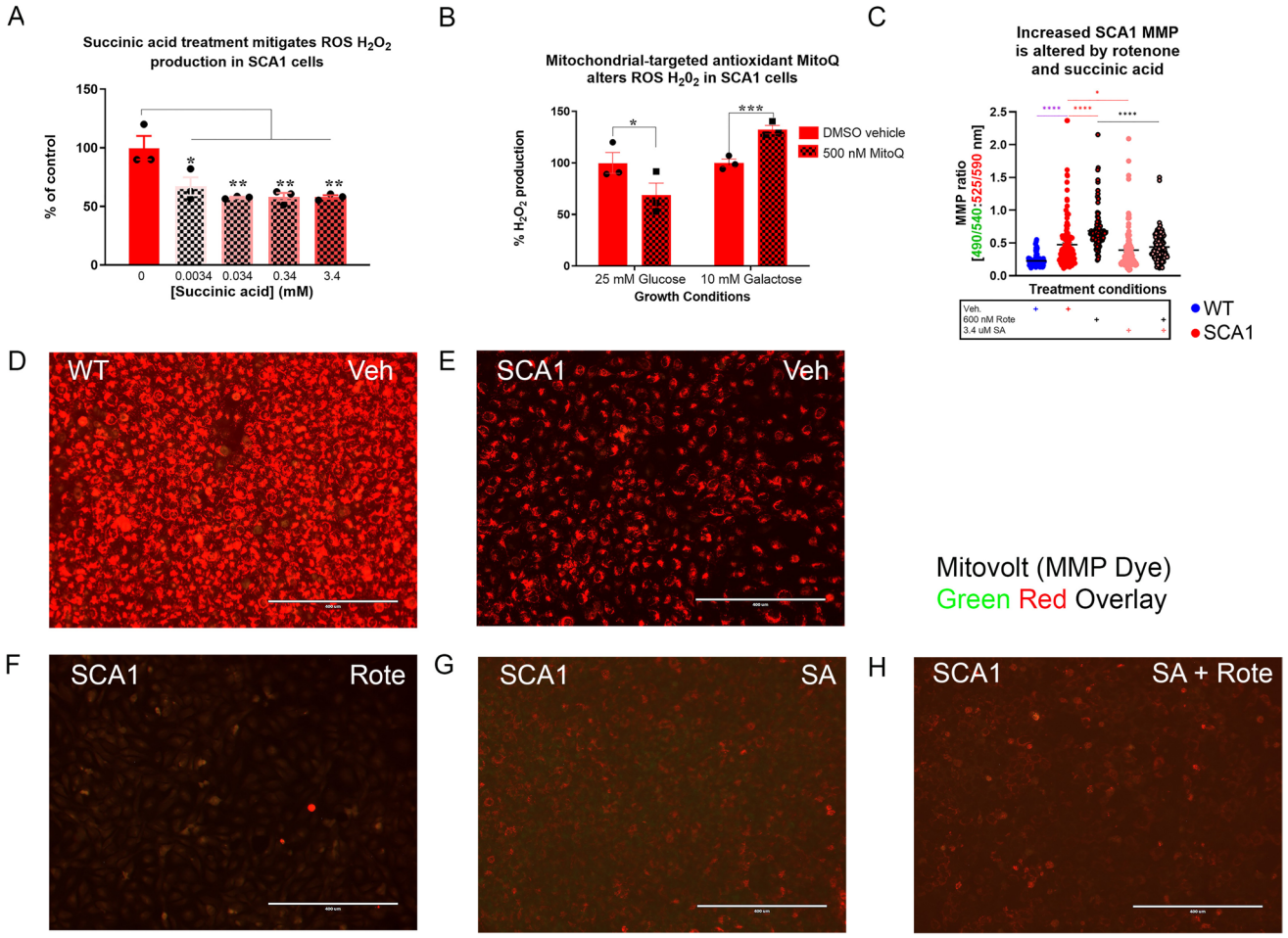

Fig. 6 Mitochondrial-targeted compounds alter the cellular and mitochondrial physiological deficits of SCA1 cells. **A** Treatment of SCA1 cells with OXPHOS complex II substrate succinic acid reduces H_2O_2 ROS production. **B** Under high (25 mM) glucose conditions, H_2O_2 ROS production in SCA1 cells can be significantly decreased with the addition of the mitochondrial-targeted antioxidant, MitoQ. Under high (10 mM) galactose conditions, MitoQ increases H_2O_2 ROS production in SCA1 cells. (C-H) Green to red channel emission ratio of vehicle-treated (Veh) WT cells and SCA1 cells, and SCA1 cells treated with the OXPHOS complex I inhibitor rotenone (Rote), succinic acid (SA) or both, was imaged and quantified. Representative green/red overlay images **C** are shown in D-H. * $P<0.05$, *** $P<0.001$, **** $P<0.0001$

stress and mitochondrial membrane potential seen in SCA1 cells. Conversely, inhibition of electron transport chain function with rotenone exacerbates mitochondrial membrane potential in the presence of ATXN1[82Q].

To assess direct interactions of mutant ATXN1 with cytoplasmic and mitochondrial proteins, we first conducted a meta-analysis of previously published data. Zhang, Williamson and Bogoyevitch (Zhang et al. 2018) developed complementary proteomics strategies (biotinylation, GFP-trap pulldown) to identify proximal (via GFP-trap pulldown) and direct (via biotinylation and GFP-trap pulldown) interactome partners of mutant ATXN1[85Q] in neuro2A cells. Both strategies were conducted under resting and oxidative stress conditions, the latter of which were induced by arsenate. We filtered their shared dataset through DAVID and MitoCarta 2.0 (Fig. 7). Three apoptotic proteins, 8 OXPHOS proteins, 8 glycolytic proteins and the mitochondrial transcription Mterf1b were identified as potential interactors of ATXN1[85Q-S776] by one of their four strategies/conditions. A combination of two of the strategies/conditions identified an additional 3 apoptotic proteins, 3 OXPHOS proteins, 3 mitochondrial membrane proteins, and 7 glycolytic proteins as potential interactors. A combination of three of the strategies/conditions identified an additional two apoptotic proteins, the mitochondrial membrane protein Slc25a12, and the glycolytic protein Galk1 as potential interactors. Finally, the mitochondrial membrane protein Slc25a31, which when mutated causes "Combined Oxidative Phosphorylation Deficiency 34" was identified as a potential interactor of ATXN1[85Q-S776] by all four proteomic strategies/conditions.

Apoptosis	OXPHOS	Mitochondrial membrane	Glycolysis	Mitochondrial transcription
Acin1	Atp5f1	Slc3a2	Acsl4	Mterf1b
Api5	Atad3a	Slc25a4	Acot7	
Bag3	Atp5l	Slc25a5	Fh1	
Bag6	Atp5c1	Slc25a31	Gapdhs	
Bclaf1	Coq6	Slc25a12	G6pdx	
Bcor	Ndufa9	Mtch2*	Galk1	
Pdcd6ip	Mthfd2		Gfpt1	
Pdcd6	Idh3a		Gfpt2	
	Idh1		Pdhb	
	Idh2		Pfkl	
			Pfkp	
			Pgls	
			Acaca	
			Acacb	
			Acadvl	
			Aco2	

Key
Rest
Stressed
Both

Fig. 7 Mutant ATXN1 interacts with and/or proximally localizes to a host of cytoplasmic and mitochondrial proteins. Filtered analysis of interactomic data from Zhang et al. 2018 (Burright et al. 1995) represents cytoplasmic and mitochondrial proteins interacting with and/or in proximity of mycBioID-ATXN1[85Q] or GFP-Trap-ATXN1[85Q] in N2a cells. Mitochondrial and glycolytic proteins that bound ATXN1[85Q] were identified through Mouse MitoCarta 2.0 cross-indexing and DAVID Functional Annotation Bioinformatics Analysis (https://david.ncicrf.gov). Proximal localization and direct interactions are shown under rest, stressed and both rest and stressed conditions. *Purkinje neuron-enriched gene

To further analyze the data, we highlighted, in blue, the combined biotinylation and GFP-trap pulldown data for cells at rest (Fig. 7). Next, we highlighted, in yellow, the combined biotinylation and GFP-trap pulldown data from the stressed condition experiments (Fig. 7). Proteins that were identified in both conditions were highlighted in green (Fig. 7). A small subset of proteins were only identified under stressed conditions indicating that the vast majority of glycolytic and mitochondrial proteins interact with ATXN1[85Q] under normal conditions.

We also investigated co-localization from z-stack slices of Mic60 and ATXN1 in WT, SCA1 and ATXN1[82Q-A776] cells. Figure 8 shows slices from the top, middle and bottom of 20 µm z-stacks of WT (A-C), SCA1 (D-F) and ATXN1[82Q-A776] cells (G-I) stained with 11NQ, Mic60 and DAPI. In all three cell types, co-localization is visible in the middle z-layers (B,E,H). However, the degree of co-localization is reduced in WT cells (A-C), compared to SCA1 cells (D-F) and ATXN1[82Q-A776] cells (G-I). Figure 8J displays an orthogonal rotation of Fig. 8H depicting co-localization in the middle of the cell. Overall, the interactomic data and co-localization analysis indicates that mutant ATXN1 interacts proximally with cytoplasmic proteins.

Discussion

The results of the present study show evidence of widespread mitochondrial and extra-mitochondrial cytoplasmic alterations in both SCA1 mice models and in a human, cerebellar-derived, SCA1 cell model. Specifically, mitochondrial-associated gene expression, mitochondrial physiology and mitochondrial morphology are disrupted. Moreover, mitochondria exhibit dysfunction even in a cell model where ATXN1 does not form nuclear aggregates and is readily degraded, suggesting that this may be due to a cytoplasmic function of ATXN1 rather than a transcriptional effect. Our results suggest that stable overexpression of mutant ATXN1 directly triggers these alterations, likely through direct protein interactions or through altered nuclear gene expression, although confirmatory experiments such as mass spectrometry or immunoprecipitation pull-down in mouse model tissue are needed.

Cultured Daoy Cells as a SCA1 Model

Cytoplasmic deficits that occur in the intact SCA1 mouse cerebellum (Ripolone et al. 2018; Ito et al. 2015; Kim et al. 2003; Ferro et al. 2017a, 2017b; Stucki et al. 2016; Sanchez et al. 2016) may be the direct result of ATXN1[82Q] expression, but it is difficult to distinguish with certainty within the context of progressive disease and accumulating toxicity. To address if mitochondrial deficits may occur independent of a global disease context, we turned to SCA1 cultured cell models. In this model, human cerebellar-derived medulloblastoma Daoy cells were stably transfected with RFP-tagged ATXN1 constructs (Park et al. 2013; Perez Ortiz et al. 2018). Daoy cells are mitotic, and admittedly therefore, a full extrapolation of our results to neurons in an intact brain is limited. However, the mitotic nature of Daoy cells, which replicate every 33.6 h (Jacobsen et al. 1985) (ATCC), strongly

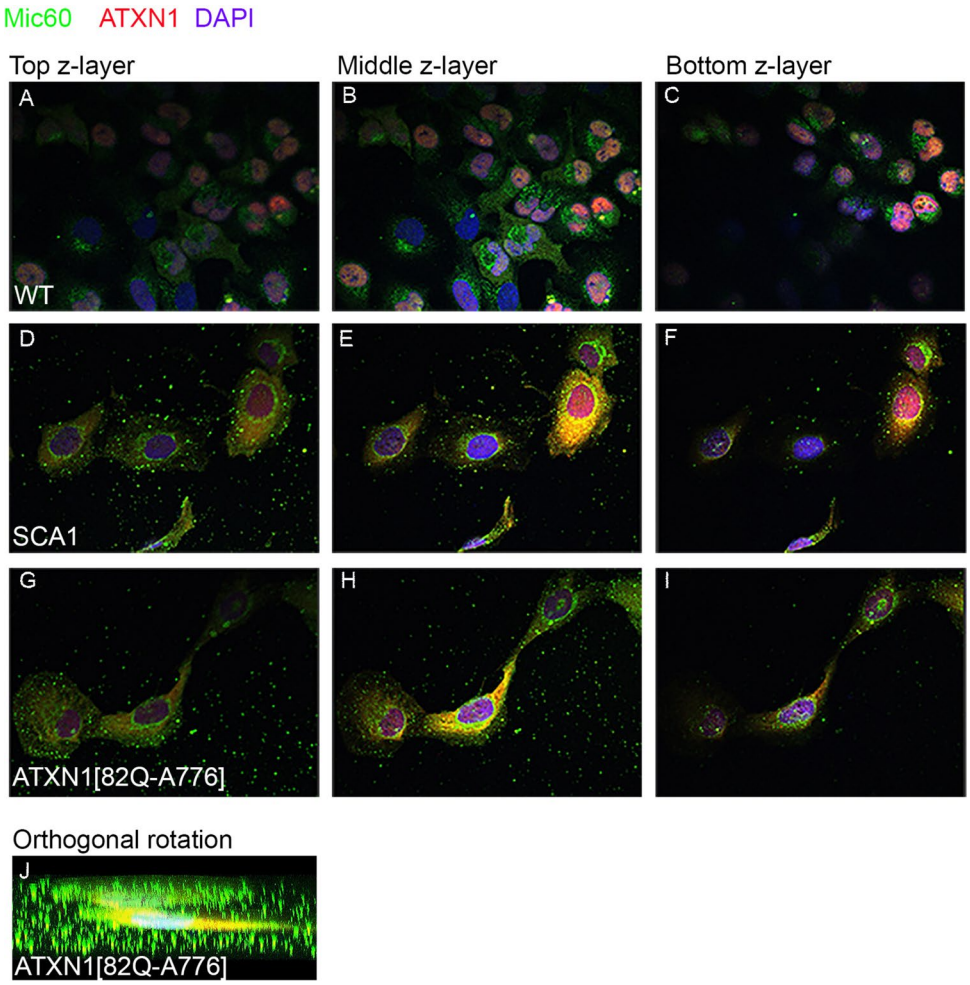

Fig. 8 Z-stack imaging of WT, SCA1 and ATXN1[82Q-A776] cells capture co-localization between the ATXN1[82Q] transgenic proteins and MICOS complex Mic60 mitochondrial protein. (**A**-**C**) Endogenous ATXN1 (red) in WT cells does not co-localize with Mic60 (green) in z-stack layers. In contrast, ATXN1[82Q] (**D**-**F**, red) and ATXN1[82Q-A776] (**G**-**I**, red) extensively co-localize (yellow) with Mic60 (green), particularly within the middle layers (**B**, **E**, **H**) of a 20 µm z-stack. (**J**) Co-localization can be seen in yellow from the rotation of the z-stack depicted in **E**

suggest that we can rule out cytoplasmic alterations as simply a secondary effect of accumulating disease toxicity. Despite such a short lifespan, expression of mutant ATXN1[82Q] in our SCA1 cell models results in significant and widespread mitochondrial and extramitochondrial cytoplasmic alterations.

Mitochondria in cells overexpressing ATXN1[82Q] display altered morphology and localization. Transmission electron micrograph (TEM) imaging of SCA1 cells reveal disrupted cristae, vacuole formation and rounded shape (Fig. 3A), indicative of a dysfunctional state common in many neurodegenerative diseases (Johri and Beal 2012). Live mitochondrial tracking analysis is needed to discern whether dysfunctional mitochondria are passed from parent to daughter cells or if new, healthy mitochondria undergo morphological changes within the short cellular lifespan. Additionally, we found through Mitotracker staining that SCA1 cells exhibiting aggregated mutant ATXN1 nuclear inclusions form perinuclear recruitment and nuclear encroachment of mitochondria (Fig. 3C), compared to SCA1 cells in which nuclear mutant ATXN1 has not yet aggregated. Recent studies have uncovered the vast extent and fluidity of mitochondrial-organelle contacts apart from the endoplasmic reticulum. Mitochondrial-nuclear contacts may represent a repair mechanism to counter localized toxicity due to aggregate formation (Savu and Moisoi 2022; Lackner 2019; Desai et al. 2020).

Physiological Deficits Due to Overexpression of ATXN1[82Q]

Physiological analysis of SCA1 models revealed decreased cellular ATP, altered ROS, enhanced bioenergetics, altered mitochondrial membrane potential function, and enhanced calcium influx. Impaired oxidative phosphorylation leads to compromised ATP production, resulting in energy deficits and neuronal dysfunction (Clemente-Suarez et al. 2023). In SCA1 cells, ATP levels were significantly reduced compared to WT cells (Fig. 5A). Production of the cell permeable reactive oxygen species H_2O_2 was measured under "control" high glucose conditions and high galactose conditions, as galactose enhances mitochondrial metabolism (Aguer et al. 2011). Our results showed that SCA1 cells under control conditions exhibited a non-significant trend of increased

H_2O_2 production compared to WT cells, an effect that was inhibited by the mitochondrial-targeted antioxidant MitoQ. Under high galactose conditions, MitoQ increased H_2O_2 production in SCA1 cells compared to untreated cells (Fig. 5B), perhaps by causing cells in high metabolism conditions to compensate by increasing H_2O_2 production in the context of enhanced elimination.

Overall bioenergetics are substantially higher in SCA1 cells compared to WT cells despite decreased levels of cellular ATP, likely reflecting the trend towards increased ROS production. More specifically, SCA1 cells displayed higher extracellular acidification rates (ECAR, measure of glycolysis) and higher oxygen consumption rates (OCR, measure of oxidative phosphorylation) compared to WT cells (Fig. 5B). Notably, ATXN1[82Q-A776] cells displayed an intermediate phenotype by exhibiting intermediate levels of basal respiration (higher in SCA1 cells than WT cells; top bar graph), proton leak (higher in SCA1 cells than WT cells; middle bar graph) and coupling efficiency of oxidative phosphorylation (lower in SCA1 cells than WT cells; lower bar graph) (Fig. 5). Although the ATXN1[82Q-A776] protein is largely degraded prior to entering the nucleus (Emamian et al. 2003), overall bioenergetics are still altered. We therefore cannot rule out the possibility that the ATXN1[82Q-A776] protein is having direct interactions with components of the cytoplasm.

Mitochondrial membrane potential (MMP) dynamics is lowered in SCA1 cells in stress conditions compared to control cells undergoing stress. MMP is a key indicator of mitochondrial activity. Specifically, a high mitochondrial membrane potential (characterized by aggregated, red/orange JC-10 dye) reflects increased proton production due to enhanced electron transport and oxidative phosphorylation, as well as mitochondrial membrane damage (Kuznetsov et al. 2008). Lowered mitochondrial membrane potential (characterized by monomeric green JC-10 dye) reflects an initiation of apoptosis combined with cytochrome C release into the cytoplasm (Kinnally and Antonsson 2007). Our results show that MMP imaging across all three cell lines at rest did not differ, likely due to the similarity of their cancerous phenotype. Induction of cellular/apoptotic stress with STR, however, uncovered a vulnerability by SCA1 cells compared to either control phenotype (Fig. 5E).

Whole cell activity was assessed by Fluo4-AM tracking of calcium influx. Following pre-treatment with DMSO vehicle, mutant ATXN1[82Q]-expressing cells display enhanced Ca^{2+} influx compared to WT cells. After inducing stress with STR, calcium levels increased considerably in the SCA1 cells compared to WT.

Direct Interactions with Mitochondrial Proteins

Our results suggest that mutant ATXN1[82Q], a very stable form of ATXN1, is directly interacting with mitochondrial proteins, and contributing to overall mitochondrial dysfunction. Specifically, our data shows altered expression of Opa1, MFN2 and TOM20 in the SCA1 and ATXN1[82Q-A776] cell lines (Fig. 4D). As previously mentioned, the ATXN1[82Q-A776] cells express an unstable form of the expanded mutant protein (Emamian et al. 2003) in addition to endogenous Daoy ATXN1. Although the ATXN1[82Q-A776] protein is substantially degraded cytoplasmically prior to entering the nucleus (Lai et al. 2011), mitochondrial proteins MFN2 and TOM20 display altered expression, indicating that it is direct cytoplasmic interaction, and not nuclear transcriptional regulation, by which ATXN1[82Q-A776] is affecting mitochondrial protein expression levels. Supporting this hypothesis is the interactomic data by Zhang and colleagues (Zhang et al. 2018) revealing in vitro, that cytoplasmic proteins interact with ATXN1[85Q] in N2A cells (Fig. 7). Overall, the data reveals that mutant ATXN1 interacts with mitochondrial proteins involved in apoptosis, oxidative phosphorylation, membrane composition and transcription, as well as with cytoplasmic glycolytic proteins. Confocal co-localization of Mic60 and cytoplasmic ATXN1, within the middle layers of the cell (Fig. 8), further support direct interaction.

Therapeutic Potential

The cumulative evidence of mitochondrial dysfunction in neurodegenerative diseases, especially that of polyglutamine-mediated disorders, requires a better understanding of mitochondrial dysfunction as a whole. Furthermore, due to the mass of evidence of neurodegenerative disease pathogenesis involving mitochondria, it could potentially provide pharmacological targets to treat many neurodegenerative diseases. In a previous study, our lab found that succinic acid boosts cerebellar function in the SCA1 B05 mouse following short-term treatment (Ferro et al. 2017a, 2017b).

Taken together, our results strongly suggest a direct interaction between mutant ATXN1 and mitochondria that lead to widespread mitochondrial and cellular alterations. Moreover, there is a growing body of evidence that pharmaceutical targeting of mitochondria may have therapeutic potential to slow down the progression of SCA1 (Ferro et al. 2017a, 2017b; Stucki et al. 2016). Due to the non-specific nature of mitochondrial dysfunction, mitochondrial-targeted drugs may have therapeutic potential beyond SCA1 as mitochondrial dysfunction is an early, non-specific symptom of many neurodegenerative diseases. While genetic, personalized therapies have a great deal of value, non-specific, small molecule therapies that slow progression may be more accessible.

Acknowledgements The authors would like to thank Dr. Harry T. Orr at the University of Minnesota for his gift of the B05 mice and 11NQ ataxin-1 antibody, Dr. Huda Zoghbi at the Baylor College of Medicine for her gift of stably-transfected Daoy cell lines, Dr. David Domozych and Lily Kozel of the Skidmore College McGraw Microscopy Center for their help with training undergraduate students on the instruments, and Sarah Thomas from Evident Scientific for live imaging experimention during our Fluoview 3000 demonstration period.

Author Contributions D.F-R, M.D., A.G., A.G., J.Y., E.L., D.N., L.S., G.B., L.K., A.F. and S.L. collected and analyzed experimental data. S.L. and J.B. oversaw experimental data collection. S.L. wrote and revised the narrative text. A.F. revised and edited the narrative text.

Data Availability No datasets were generated or analysed during the current study.

Declarations

Competing interests The authors declare no competing interests.

References

Aguer C et al (2011) *Ga*lactose enhances oxidative metabolism and reveals mitochondrial dysfunction in human primary muscle cells. PLoS ONE 6:e28536. https://doi.org/10.1371/journal.pone.0028536

Burright EN et al (1995) *SC*A1 transgenic mice: a model for neurodegeneration caused by an expanded CAG trinucleotide repeat. Cell 82:937–948

Burright EN, Orr HT, Clark HB (1997) Mouse models of human CAG repeat disorders. Brain Pathol 7:965–977

Chen HK et al (2003) Interaction of Akt-phosphorylated ataxin-1 with 14–3-3 mediates neurodegeneration in spinocerebellar ataxia type 1. Cell 113:457–468

Chung MY et al (1993) Evidence for a mechanism predisposing to intergenerational CAG repeat instability in spinocerebellar ataxia type I. Nat Genet 5:254–258. https://doi.org/10.1038/ng1193-254

Clark HB, Orr HT (2000) Spinocerebellar ataxia type 1–modeling the pathogenesis of a polyglutamine neurodegenerative disorder in transgenic mice. J NEuropathol Exp Neurol 59:265–270

Clark HB et al (1997) *Pu*rkinje cell expression of a mutant allele of SCA1 in transgenic mice leads to disparate effects on motor behaviors, followed by a progressive cerebellar dysfunction and histological alterations. J NEurosci 17:7385–7395

Clemente-Suarez VJ et al (2023) *Mi*tochondria and brain disease: a comprehensive review of pathological mechanisms and therapeutic opportunities. BioMedicines. https://doi.org/10.3390/biomedicines11092488

Cummings CJ et al (1998) Chaperone suppression of aggregation and altered subcellular proteasome localization imply protein misfolding in SCA1. Nat Genet 19:148–154. https://doi.org/10.1038/502

Cummings CJ et al (1999) Mutation of the E6-AP ubiquitin ligase reduces nuclear inclusion frequency while accelerating polyglutamine-induced pathology in SCA1 mice. Neuron 24:879–892

de Chiara C, Menon RP, Strom M, Gibson TJ, Pastore A (2009) Phosphorylation of S776 and 14–3-3 binding modulate ataxin-1 interaction with splicing factors. PLoS ONE 4:e8372. https://doi.org/10.1371/journal.pone.0008372

Desai R et al (2020) *Mi*tochondria form contact sites with the nucleus to couple prosurvival retrograde response. Sci Adv. https://doi.org/10.1126/sciadv.abc9955

Emamian ES et al (2003) *Se*rine 776 of ataxin-1 is critical for polyglutamine-induced disease in SCA1 transgenic mice. Neuron 38:375–387

Ferro A et al (2017) *Tr*eating SCA1 Mice with Water-Soluble Compounds to Non-Specifically Boost Mitochondrial Function. J Vis Exp. https://doi.org/10.3791/53758

Ferro A et al (2017b) *Sh*ort-term succinic acid treatment mitigates cerebellar mitochondrial OXPHOS dysfunction, neurodegeneration and ataxia in a Purkinje-specific spinocerebellar ataxia type 1 (SCA1) mouse model. PLoS ONE 12:e0188425. https://doi.org/10.1371/journal.pone.0188425

Huang H et al (2022) *In*tercellular propagation and aggregate seeding of mutant Ataxin-1. J MOl Neurosci 72:708–718. https://doi.org/10.1007/s12031-021-01944-1

Ingram M et al (2016) *Ce*rebellar transcriptome profiles of ATXN1 transgenic mice reveal SCA1 disease progression and protection pathways. Neuron 89:1194–1207. https://doi.org/10.1016/j.neuron.2016.02.011

Irwin S et al (2005) *R*NA association and nucleocytoplasmic shuttling by ataxin-1. J Cell Sci 118:233–242. https://doi.org/10.1242/jcs.01611

Ito H et al (2015) *HM*GB1 facilitates repair of mitochondrial DNA damage and extends the lifespan of mutant ataxin-1 knock-in mice. EMBO Mol Med 7:78–101. https://doi.org/10.15252/emmm.201404392

Jacobsen PF, Jenkyn DJ, Papadimitriou JM (1985) Establishment of a human medulloblastoma cell line and its heterotransplantation into nude mice. J NEuropathol Exp Neurol 44:472–485. https://doi.org/10.1097/00005072-198509000-00003

Johri A, Beal MF (2012) Mitochondrial dysfunction in neurodegenerative diseases. J PHarmacol Exp Ther 342:619–630. https://doi.org/10.1124/jpet.112.192138

Jorgensen ND et al (2007) *Hs*p70/Hsc70 regulates the effect phosphorylation has on stabilizing ataxin-1. J NEurochem 102:2040–2048. https://doi.org/10.1111/j.1471-4159.2007.04678.x

Jorgensen ND et al (2009) Phosphorylation of ATXN1 at Ser776 in the cerebellum. J Neurochem 110:675–686. https://doi.org/10.1111/j.1471-4159.2009.06164.x

Kim SJ et al (2003) *Po*lyglutamine-expanded ataxin-1 recruits Cu/Zn-superoxide dismutase into the nucleus of HeLa cells. BioChem Biophys Res Commun 307:660–665. https://doi.org/10.1016/s0006-291x(03)01241-5

Kinnally KW, Antonsson B (2007) A tale of two mitochondrial channels, MAC and PTP, in apoptosis. Apoptosis 12:857–868. https://doi.org/10.1007/s10495-007-0722-z

Kraus-Perrotta C, Lagalwar S (2016) Expansion, mosaicism and interruption: mechanisms of the CAG repeat mutation in spinocerebellar ataxia type 1. Cerebellum Ataxias 3:20. https://doi.org/10.1186/s40673-016-0058-y

Kuznetsov AV et al (2008) *An*alysis of mitochondrial function in situ in permeabilized muscle fibers, tissues and cells. Nat Protoc 3:965–976. https://doi.org/10.1038/nprot.2008.61

Lackner LL (2019) The expanding and unexpected functions of mitochondria contact sites. TreNds Cell Biol 29:580–590. https://doi.org/10.1016/j.tcb.2019.02.009

Lagalwar S (2022) Mechanisms of tunneling nanotube-based propagation of neurodegenerative disease proteins. FroNt Mol Neurosci 15:957067. https://doi.org/10.3389/fnmol.2022.957067

Lai S, O'Callaghan B, Zoghbi HY, Orr HT (2011) 14–3-3 Binding to ataxin-1(ATXN1) regulates its dephosphorylation at Ser-776 and transport to the nucleus. J Biol Chem 286:34606–34616. https://doi.org/10.1074/jbc.M111.238527

Lim J et al (2006) A protein-protein interaction network for human inherited ataxias and disorders of Purkinje cell degeneration. Cell 125:801–814. https://doi.org/10.1016/j.cell.2006.03.032

Lim J et al (2008) Opposing effects of polyglutamine expansion on native protein complexes contribute to SCA1. Nature 452:713–718. https://doi.org/10.1038/nature06731

Matilla-Dueñas A, Goold R, Giunti P (2008) Clinical, genetic, molecular, and pathophysiological insights into spinocerebellar ataxia type 1. Cerebellum 7:106–114. https://doi.org/10.1007/s12311-008-0009-0

Orr HT et al (1993) Expansion of an unstable trinucleotide CAG repeat in spinocerebellar ataxia type 1. Nat Genet 4:221–226. https://doi.org/10.1038/ng0793-221

Park J et al (2013) RAS-MAPK-MSK1 pathway modulates ataxin 1 protein levels and toxicity in SCA1. Nature 498:325–331. https://doi.org/10.1038/nature12204

Perez Ortiz JM et al (2018) Reduction of protein kinase A-mediated phosphorylation of ATXN1-S776 in Purkinje cells delays onset of ataxia in a SCA1 mouse model. NEurobiol Dis 116:93–105. https://doi.org/10.1016/j.nbd.2018.05.002

Ripolone M et al (2018) *Pu*rkinje cell COX deficiency and mtDNA depletion in an animal model of spinocerebellar ataxia type 1. J NEurosci Res 96:1576–1585. https://doi.org/10.1002/jnr.24263

Sanchez I, Balague E, Matilla-Duenas A (2016) Ataxin-1 regulates the cerebellar bioenergetics proteome through the GSK3beta-mTOR pathway which is altered in spinocerebellar ataxia type 1 (SCA1). Hum Mol Genet 25:4021–4040. https://doi.org/10.1093/hmg/ddw242

Savu DI, Moisoi N (2022) Mitochondria - Nucleus communication in neurodegenerative disease. Who talks first, who talks louder? Biochimica Et Biophysica Acta (BBA) 1863:148588. https://doi.org/10.1016/j.bbabio.2022.148588

Schut J, Haymaker W (1951) A pathologic study of five cases of common ancestry. Jneuropath Clin Neurol 1:183–213

Serra HG et al (2006) RORalpha-mediated Purkinje cell development determines disease severity in adult SCA1 mice. Cell 127:697–708. https://doi.org/10.1016/j.cell.2006.09.036

Servadio A et al (1995) Expression analysis of the ataxin-1 protein in tissues from normal and spinocerebellar ataxia type 1 individuals. Nat Genet 10:94–98. https://doi.org/10.1038/ng0595-94

Stucki DM et al (2016) *Mi*tochondrial impairments contribute to spinocerebellar ataxia type 1 progression and can be ameliorated by the mitochondria-targeted antioxidant MitoQ. Free Radic Biol Med 97:427–440. https://doi.org/10.1016/j.freeradbiomed.2016.07.005

Vandaele S et al (1991) *Pu*rkinje cell protein-2 regulatory regions and transgene expression in cerebellar compartments. GenEs Dev 5:1136–1148

Yue S, Serra HG, Zoghbi HY, Orr HT (2001) The spinocerebellar ataxia type 1 protein, ataxin-1, has RNA-binding activity that is inversely affected by the length of its polyglutamine tract. Hum Mol Genet 10:25–30. https://doi.org/10.1093/hmg/10.1.25

Zhang S, Williamson NA, Bogoyevitch MA (2018) Complementary proteomics strategies capture an ataxin-1 interactome in Neuro-2a cells. Sci Data 5:180262. https://doi.org/10.1038/sdata.2018.262

Zoghbi HY, Orr HT (2009) Pathogenic mechanisms of a polyglutamine-mediated neurodegenerative disease, spinocerebellar ataxia type 1. J Biol Chem 284:7425–7429. https://doi.org/10.1074/jbc.R800041200